Co-actuation: Achieve High Stiffness and Low Inertia in Force Feedback Device

Jian Song, Yuru Zhang(✉), Hongdong Zhang,
and Dangxiao Wang(✉)

Beihang University, No. 37 Xueyuan Rd., Haidian, Beijing, China
{yuru, hapticwang}@buaa.edu.cn

Abstract. Achieving high stiffness, low inertia and friction is a big challenge in the design of a haptic device. Admittance display is a common solution to obtain high stiffness but is difficult to achieve low inertia and friction. We describe a new concept of co-actuation to overcome this difficulty. The co-actuation approach disconnects the actuators and joints of a haptic device, making the two components work cooperatively according to characteristics of simulated environment. In free space, the joints are tracked and followed by the actuators. Users can move the joints freely without feeling resistance from the actuators. In constraint space, physical constraints driven by the actuators apply impedance to the joints. By producing a direct physical contact between the joints and the physical constraints, users can feel a hard virtual surface. The paper describes the mechanical and control design and implementation of a one degree-of-freedom (DOF) co-actuation module. Stiffness of 40 N/mm and friction force of less than 0.3 N was achieved on the module. By effectively reducing inertia and friction, the proposed approach demonstrates its potential advantage over conventional admittance displays. The co-actuation approach can be applied to multi-DOF haptic devices to achieve high stiffness, low inertia and friction.

Keywords: Co-actuation · Haptic device · High stiffness · Low inertia

1 Introduction

It is well known that impedance displays and admittance displays are two distinct classes of haptic devices. Impedance displays usually have low inertia and friction, and are highly back-drivable [1, 2]. Admittance displays usually contain a transmission of significant reduction, and are therefore non-back-drivable due to high inertia and friction [3, 4]. The essential control paradigm of impedance displays is displacement in, and force out. Admittance control is the inverse of impedance control. Although well-engineered admittance devices may have a higher dynamic range than their counterparts, most successful commercial haptic displays are impedance devices [5].

Impedance displays and admittance displays are dual not only in their cause-and-effect structure, but also in their performance and limitation. Impedance devices typically are able to display low-inertia, low-damping environments, but have difficulty rendering stiff constraints. Notable impedance devices, Phantom models, have a maximum stable stiffness range from 1 to 3.5 N/mm [6]. Admittance devices on the other hand are capable of rendering high stiffness and high force. However, they are

© Springer International Publishing Switzerland 2016
F. Bello et al. (Eds.): EuroHaptics 2016, Part I, LNCS 9774, pp. 229–239, 2016.
DOI: 10.1007/978-3-319-42321-0_21

often not capable of rendering low inertia. Notable admittance device, Haptic Master, has a stable stiffness range from 10–50 N/mm and the nominal/max force are 100/250 N, while the minimal tip inertia is 2 kg [3]. In some applications, such as dental surgery simulation [7], both low inertia and high stiffness are required to render light dental tools and rigid tooth surfaces. Either conventional impedance display or admittance display are difficult to achieve the required performances.

Our goal is to develop a new haptic device that can render both low inertia and high stiffness for potential application in dental simulation. To achieve the goal, we need to overcome the limitations of impedance displays in rendering high stiffness and admittance displays in rendering low inertia. We adopt the principle of admittance display to achieve high stiffness. To overcome the limitation of high inertia and friction, we introduce a new concept of co-actuation. The basic idea of co-actuation is to disconnect the joints with their actuators in a haptic device. The actuators will follow the motion of the joints and apply required force when necessary. Because the actuators and the joints are separated, the inertia and friction in the actuators and its transmission will not be reflected to the device. Therefore, it is possible for the co-actuation approach to achieve high stiffness at the level of admittance displays while keep low inertia and friction at the level of impedance displays. In this paper, we describe the co-actuation approach by the design and construction of a single DOF haptic interface prototype. Our work is primarily inspired by the prior work on dynamic physical constraint (DPC) [8].

2 Related Works

The emulation of hard virtual surface has led to numerous research efforts. Different concepts have been tried in order to implement a truly "hard" constraint. Several researchers studied the maximum stiffness that an impedance display can stably render. Colgate and Schenkel developed a relationship between damping, stiffness, and update rate from which the maximum stiffness of a virtual wall can be estimated [9]. More recently, the relationship was generalized by considering more factors including sensor quantization and coulomb friction [10–12].

To render stiff environments over a large workspace, Zinn *et al.* [13] addressed the limitation of traditional impedance devices by introducing a new actuation approach based on parallel actuation concept. They divided the torque generation into separate low and high-frequency actuators whose torque sum in parallel. A high-power, high-torque actuator was used to provide the low frequency torques while a small, fast actuator was used to provide the high frequency torques. They also distributed the low and high-frequency actuators to locations on the device so that their effect on device transparency was minimized while their contribution to force dynamic range was maximized. Experimental data showed that the approach was able to achieve a high stiffness of 57 N/mm for a three DOF prototype and reduce the output friction to less than 1.5 N within a large workspace of 0.6 m^3.

Since brakes are dissipative by nature, they are ideally suited to provide physical damping for a haptic device. Several researchers have investigated the use of brakes to achieve high impedance and thus improve stability. Different types of brakes were used

[14–18]. It was found that some characteristics of the brakes, such as slow to actuate and nonlinear relationship between velocity and torque, limit the fidelity of the rendering. To improve the performance, Gosline and Hayward proposed to use eddy current brakes (ECBs) as linear, fast actuating, programmable viscous dampers for haptic rendering. They found that virtual walls rendered using the physical dampers do not have the characteristic "sticky" feel that is typical of walls rendered using conventional programmable brakes. However, the use of dampers in brakes leads to increase in the inertia and power consumption of the device [19]. In an alternative approach, the dissipative properties of a DC motor were taken as an advantage to realize programmable electrical damping [20].

Another concept to provide a convincingly hard surface is to use mechanical constraints. A typical example was Cobot, which used parallel linkage to build a 6 DOF device [4]. Although controlled as an admittance device, the Cobot does not suffer from the high inertia, friction and backlash that normally exist in a highly geared admittance device. By using a rotational-to-linear continuously variable transmission (CVT), the Cobot enhanced dynamic range that extends continuously from a completely clutched state to a highly back drivable state. With the novel mechanical design, the Cobot achieved a force transmission capabilities exceeding 50 N, structural stiffness ranging from 20–400 N/mm, a motion control bandwidth of 40 Hz, and near zero power requirements for sustaining high output loads.

A further variation on mechanical constraints is dynamic physical constraints (DPC) introduced recently by [8]. The DPC is adjusted depending on the user's current position in space. When not in contact with the virtual surface, the user can move the device with complete freedom as all joints are unimpeded. Once the virtual surface is reached, the DPC creates a unidirectional physical barrier to limit the movement of partial joints. The DPC concept can produce a realistic sensation of hard surface contact because of the real physical contact between the user and the DPC. However, the DPC concept was proposed to emulate a virtual surface that is approximately concentric with the central pivot point. The extension of this idea to arbitrary virtual surfaces needs further investigation.

3 Principle of Co-actuation

To render realistic virtual environments, the difference between desired and rendered dynamics must be small. We focus on a virtual environment in surgical simulation in which a light surgical tool is required to interact with a stiff object. To simulate the light tool and stiff object contact, a haptic device should be able to display low inertia and high stiffness. Impedance displays are good at simulating low inertia, but suffer from instability and surface penetration problems commonly experienced with high stiffness values. In contrast, admittance displays can provide high stiffness, but are difficult to simulate low inertia. In the following, we present a new concept of co-actuation for achieving high stiffness and low inertia of a haptic device.

The key point of the co-actuation concept is to disconnect the actuators with the joints of linkage in order to reduce the inertia of the device. Figure 1 shows the concept using a one DOF co-actuation module which works in two modes: free motion and

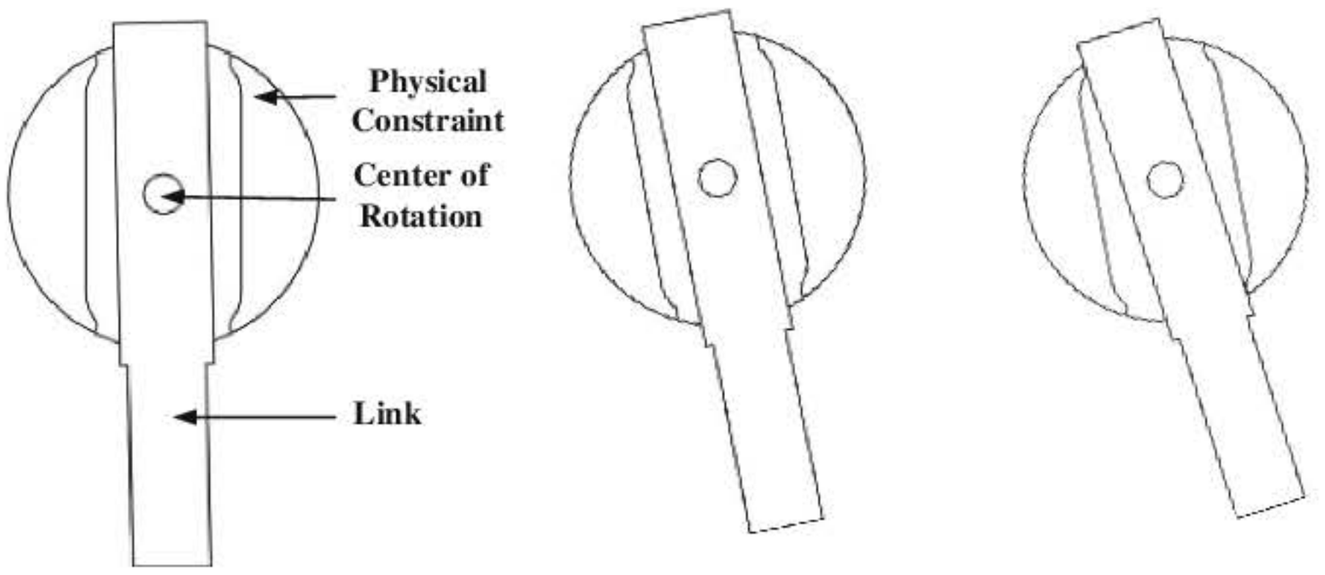

Fig. 1. One DOF co-actuation module: (a) home position; (b) free motion; (c) constrained motion.

constrained motion. In free motion mode, the rotation of link is free but tracked by the physical constraint. The motion of link is unimpeded because the physical constraint is not in contact with the link, but continually keeps a short distance with the link. In constrained motion mode, the motion of the link is impeded by the physical constraint through the physical contact between them. Because of mechanical decoupling between the joint and the motor, high stiffness can be achieved by adopting large gear reductions without affecting users' feeling in free space.

4 Mechanical Structure of a One DOF Co-actuation Module

To illustrate how the co-actuation concept can be implemented, we designed a mechanical structure for the co-actuation module of Fig. 1. As shown in Fig. 2a, two optical encoders are placed on the joint axis and the motor axis respectively. A force sensor is mounted at the tip of the link to measure the force applied by the user. The physical constraint is actuated by a motor connected to a high-ratio gear reducer and controlled by a two-mode controller described in the next section. During free motion, the joint angle of the link is measured to command the tracking motion of the physical

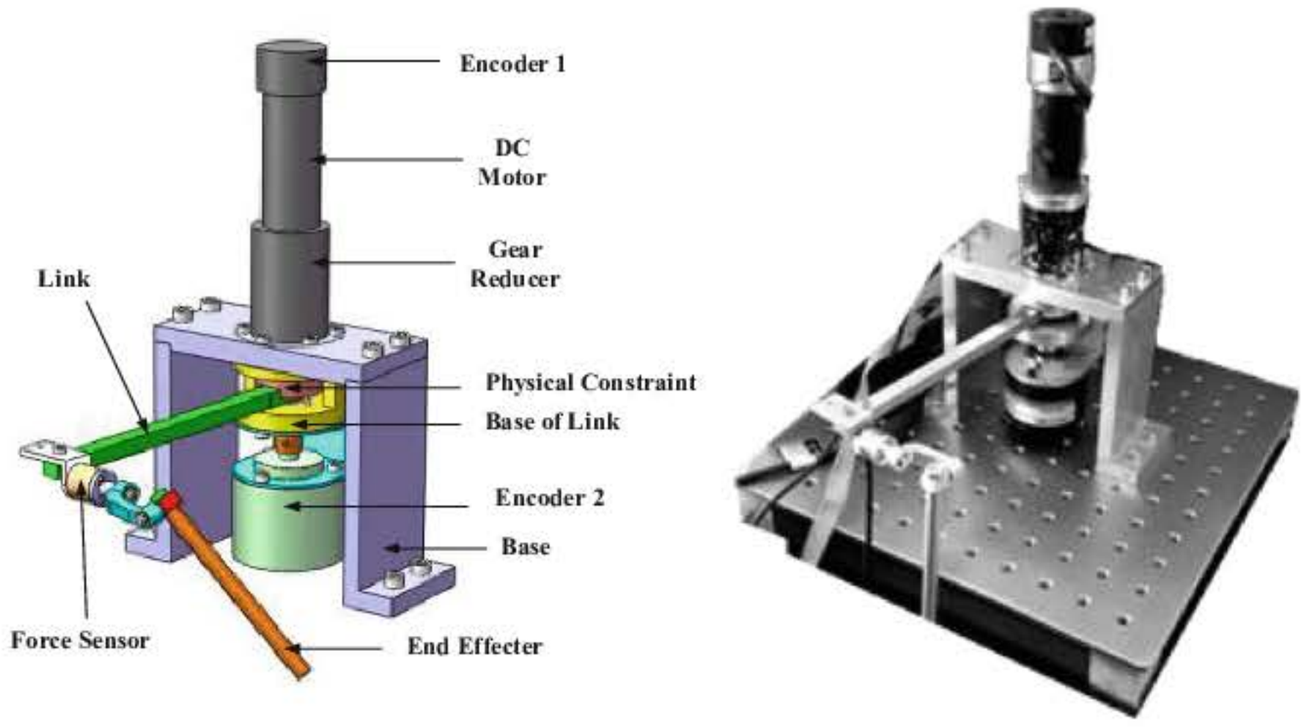

a) virtual prototype b) physical prototype

Fig. 2. Structure of a one DOF co-actuation module

constraint. During constraint motion, the user's force is measured to command the reactive force of the physical constraint.

A clearance between the link and the physical constraint is designed to obtain decouple between the link and the actuator, and also to allow the encoder of the joint to detect the link motion. The amount of the clearance depends on the speed of the link and the frequency response of the motor. In general, the higher the speed and the lower the frequency response, the larger the clearance should be. However, if the clearance is bigger, the switch between free space and constrained space requires a longer time, which may decrease the performance of stiff object simulation. For high stiffness performance, it is ideal that the clearance is zero so that the switch between free space and constrained space requires no time. Therefore, the critical problem in the design of the co-actuation module is to find a minimum clearance by making a tradeoff between the performances in free space and constraint space. This problem will be addressed in the next section on the control approach of co-actuation.

5 Control Approach of Co-actuation

5.1 Control Structure for Co-actuation

Figure 3 shows the control structure for the co-actuation module. By decomposing the actuator and joint, the co-actuation module can achieve a high transparency in free space and high stiffness in constraint space. Users can move the link freely when in free space as the joint is unimpeded by friction and inertia of the motor and reducer. In constraint space, users can feel a hard virtual surface due to the direct physical contact between the link and the physical constraint. The co-actuation module can apply bidirectional impedance to the joint, which is different from the DPC concept [8]. This characteristic

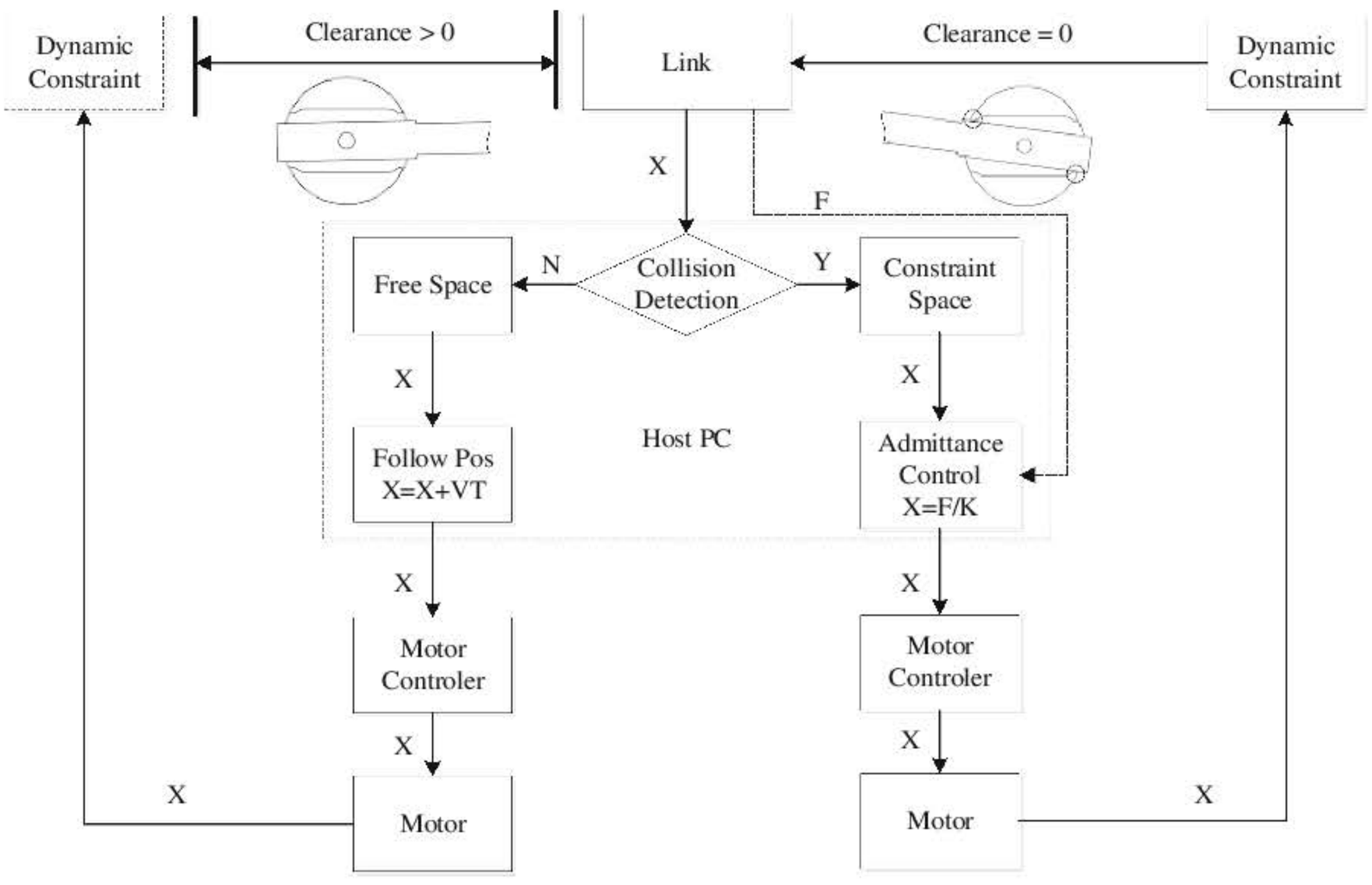

Fig. 3. Control architecture of co-actuation

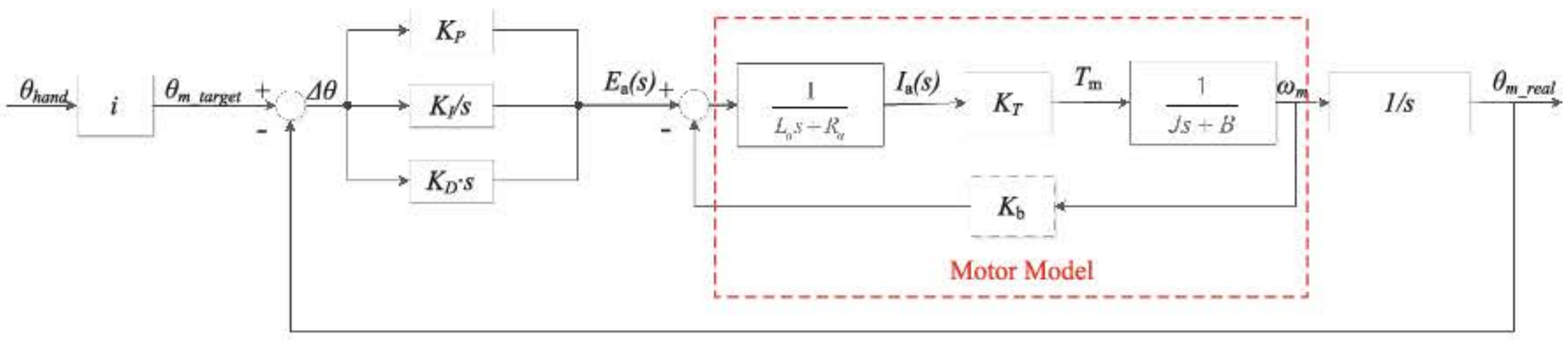

Fig. 4. Block diagram of the control loop

makes the co-actuation concept capable of emulating arbitrary hard surfaces and extended to broaden the range of applications. Force sensors are needed to predict the user's intent, which means that admittance control method is used in constraint space.

5.2 Clearance Model

The diagram shown in Fig. 4 illustrated the control law in the free space, which was used to derive the clearance model to maintain the movement of the actuator to follow the movement of the link. i refers to the gear ratio.

The transfer function of the control loop can be derived as

$$H(s) = [\theta_{m\_real}(s)]/[\theta_{hand}(s)] = \frac{PID(s)M(s)}{PID(s)M(s) + s} \cdot i \tag{1}$$

where $PID(s)$ and $M(s)$ refers to the transfer function of the PID controller and the motor model respectively.

Suppose the performance of the PID controller is perfect and $La \ll Ra$ for typical DC servo motors, the function becomes

$$H(s) = \frac{K_T \cdot i}{JR_a s^2 + (BR_a + K_T K_b)s + K_T} \tag{2}$$

Suppose the hand moves at the maximum velocity $\omega_{\max}$, and then we can derive

$$\theta_{hand} = \frac{\omega_{\max}}{s^2} \tag{3}$$

The maximal steady-state following error $\Delta\theta_{\max}$ should be

$$\Delta\theta_{\max} = \lim_{s \to 0} s \cdot (\theta_{hand}(s) - \theta_{m\_real}(s)/i) \tag{4}$$

Combining with Eq. (2), we can derive

$$\Delta\theta_{\max} = \frac{BR_a + K_T K_b}{K_T} \cdot \omega_{\max} \tag{5}$$

In order to ensure no contact between the link and the physical constraint, the minimal clearance $\delta_{\min}$ should follow

$$\delta_{\min} > \Delta\theta_{\max} \tag{6}$$

This model implicates that the minimal clearance is correlated with the maximal interaction velocity, the impedance of the structure, and the performance of the motor.

6 Performance Experiments

Table 1 shows the values of main parameters in the physical prototype (Fig. 2b).

Table 1. Values of main parameters in the one DOF prototype

Parameter	Value	Parameter	Value
Motor	MAXON RE30 268214	Gear reducer	Harmonic drive, Ratio 50
Res. of the motor's encoder	0.036°	Force sensor	ATI NANO17, Max F_z 70 N
Res. of the link's encoder	0.005°	Servo rate	1 kHz

6.1 Free Motion Performance

In the prototype, the clearance between the link and the physical constraint was set as 1.62°. To validate the performance of simulating free space, the user rotated the link back and forth for three times. The motor was driven to follow the motion of the link. From Fig. 5, the constraint angle followed the link angle in a responsive way, and the clearance was maintained above zero at all time. Correspondingly, the real-time back driving force measured by the force sensor was shown in Fig. 6. The average force is about 0.1 N, and the maximal force is less than 0.3 N. These results demonstrated that the prototype produced satisfied free space performance.

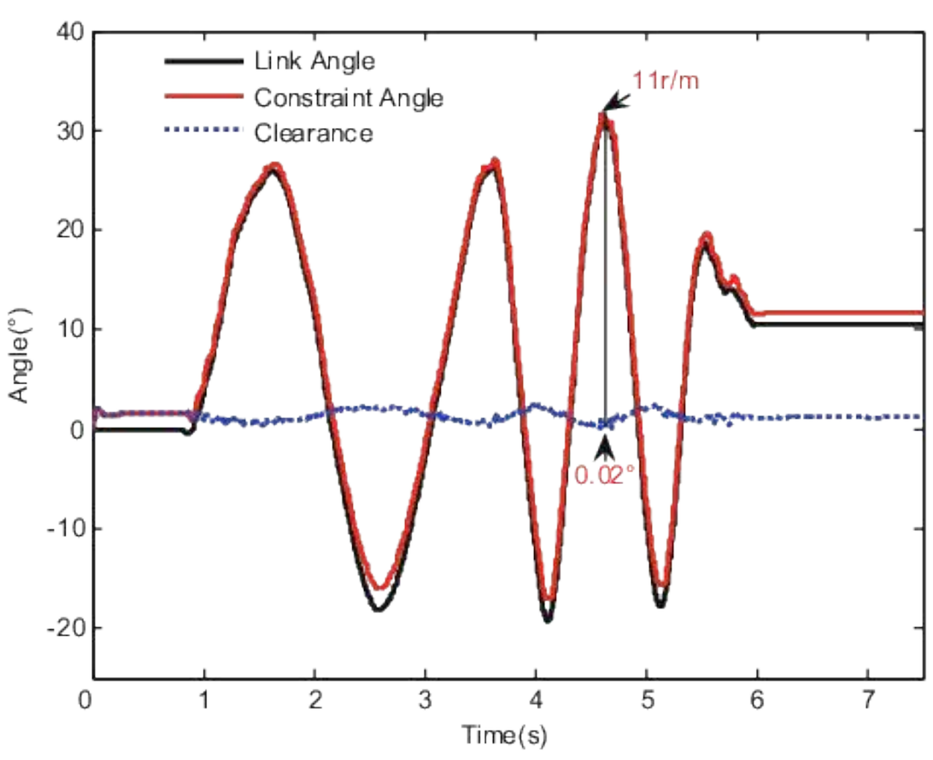

Fig. 5. High frequency accurate tracking (Color figure online)

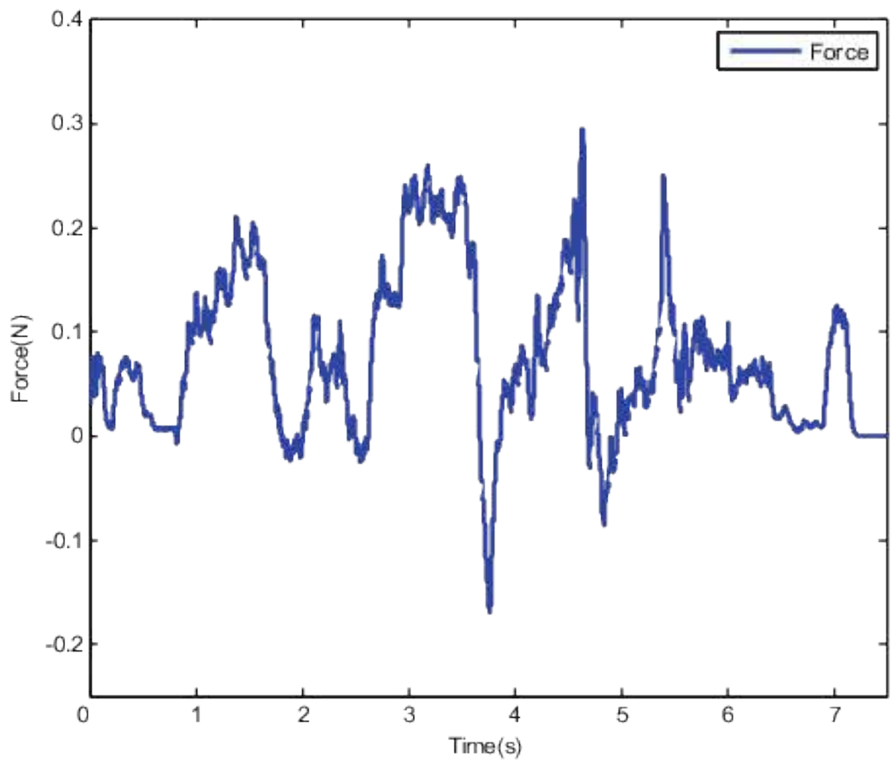

Fig. 6. Back driving force (Color figure online)

As shown in Fig. 5, the clearance between the link and the physical constraint was about 0.02° when the moving velocity of the link approached 11 rpm. Considering the model in Eq. (5), the theoretical value of $\Delta\theta_{max}$ is 1.65° when the maximum moving velocity ω_{max} is 11 rpm. The small error between the theoretical and measured value of the clearance illustrated the accuracy of the theoretical model.

6.2 Constrained Motion Experiment

To validate the performance of simulating constraint space, the user rotated the link to collide with a pre-defined virtual wall. Figure 7 illustrated the measured contact force versus the penetration distance of the link into the virtual wall. The parameter r refers to the distance (i.e. the rotating radius) from the force exerting point to the rotating center of the link. The results showed that a higher stiffness of the virtual wall can be achieved with the cost of reducing workspace of the end-effector. For the shorter rotating radius (r = 0.08 m), the workspace is sufficient for some fine manipulations such as the movement of a dental tool in an oral cavity. The measured contact stiffness (40 N/mm) provides a promising solution for simulating stiff contacts.

Another interesting finding is there existed two slopes of the stiffness for a given rotating radius. To investigate the possible reasons leading to this two-phase stiffness, we performed another experiment in which the motor was turned off in the constraint space. Therefore, when the user rotated the link to collide the actuator, he/she felt the pure mechanical resistance produced by the mechanical damping and the gear reduction system, instead of the servo-controlled virtual wall. The shaft of the motor did not rotate until the active force from the user was big enough to back-drive the motor and the gear-box. As shown in Fig. 8, the stiffness of the pure mechanical contact was identical to the first phase stiffness in the Fig. 7. This coincidence implied that the stiffness of the first phase was produced by the mechanical contact and the second phase was produced by both the mechanical and electrical impedances.

Based on above analysis, we can infer the two phase stiffness was caused by the mechanical clearance. The servo-controlled algorithm did not work until the clearance was eliminated by the increasing contact force from the user.

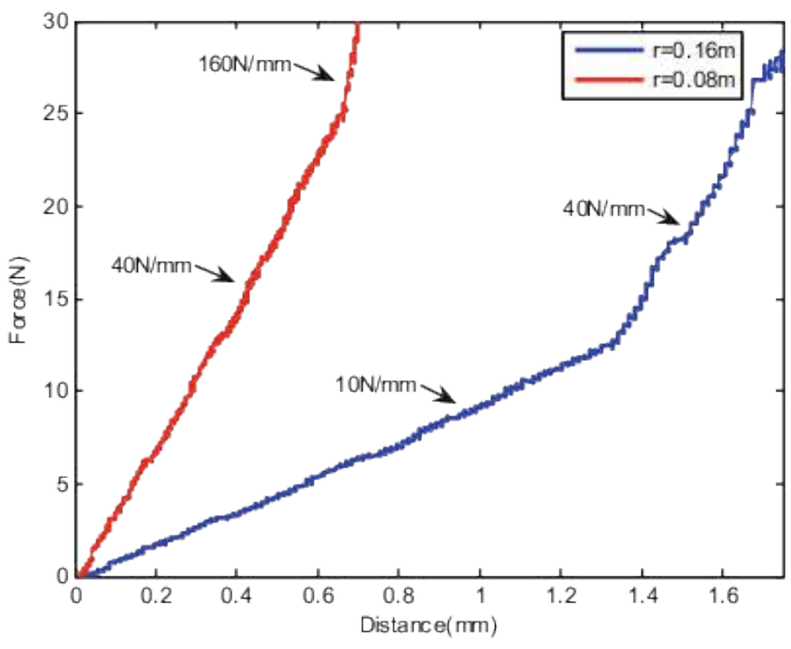

Fig. 7. Stiffness of simulating a virtual wall (Color figure online)

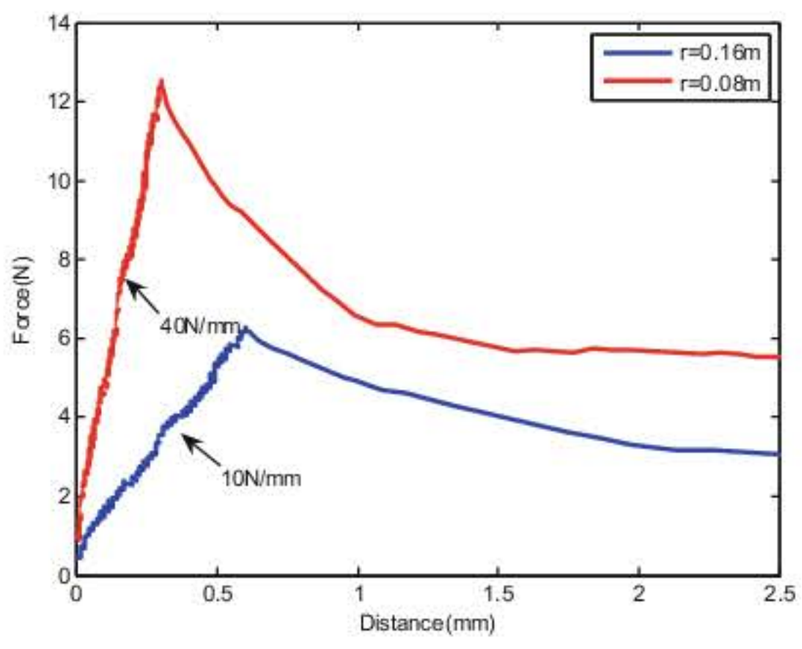

Fig. 8. Stiffness when the motor was turned off (Color figure online)

From the human perception side, Lawrence and Chapel [21] reported that stiffness greater than 10 N/mm would be difficult for humans to differentiate between, suggesting that the proposed method could be used for the realistic perception of hardness. Theoretically speaking, the first phase stiffness should be much larger as both the link and the physical constraint was made of Aluminum, which should produce large mechanical contact stiffness. However, there existed clearance in the bearing of the link's shaft, actual stiffness was greatly reduced. In the next step, a smaller tolerance in the mechanical design and assembly may help to reduce the influence of this issue.

7 Co-actuation in Multi-DOF Devices

The concept of co-actuation can be extended to multi-DOF devices. Figure 9 illustrates two examples of 3-DOF haptic devices in the cases of parallel and serial linkages. In each case, we can obtain a multi-DOF haptic device by simply use the co-actuation module described in Sect. 4 for each active joint of the linkage. A particular issue needs to be considered is the increase in inertia of a multi-DOF haptic device. In the case of parallel linkage, even though the effective inertia of the device does not include the inertia of actuation, the linkage itself might be too heavy due to a large number of links. The same problem is more sever in the case of serial linkage, because most co-actuation modules are located in the moving links and their inertia will affect the effective inertia of the haptic device. Although the problem of increased inertia may limit the application of the co-actuation method, it is possible to include gravity compensation in the co-actuation module to obtain good transparency in free space. When the gravity compensation is necessary, the co-actuation module works like an admittance-controlled device.

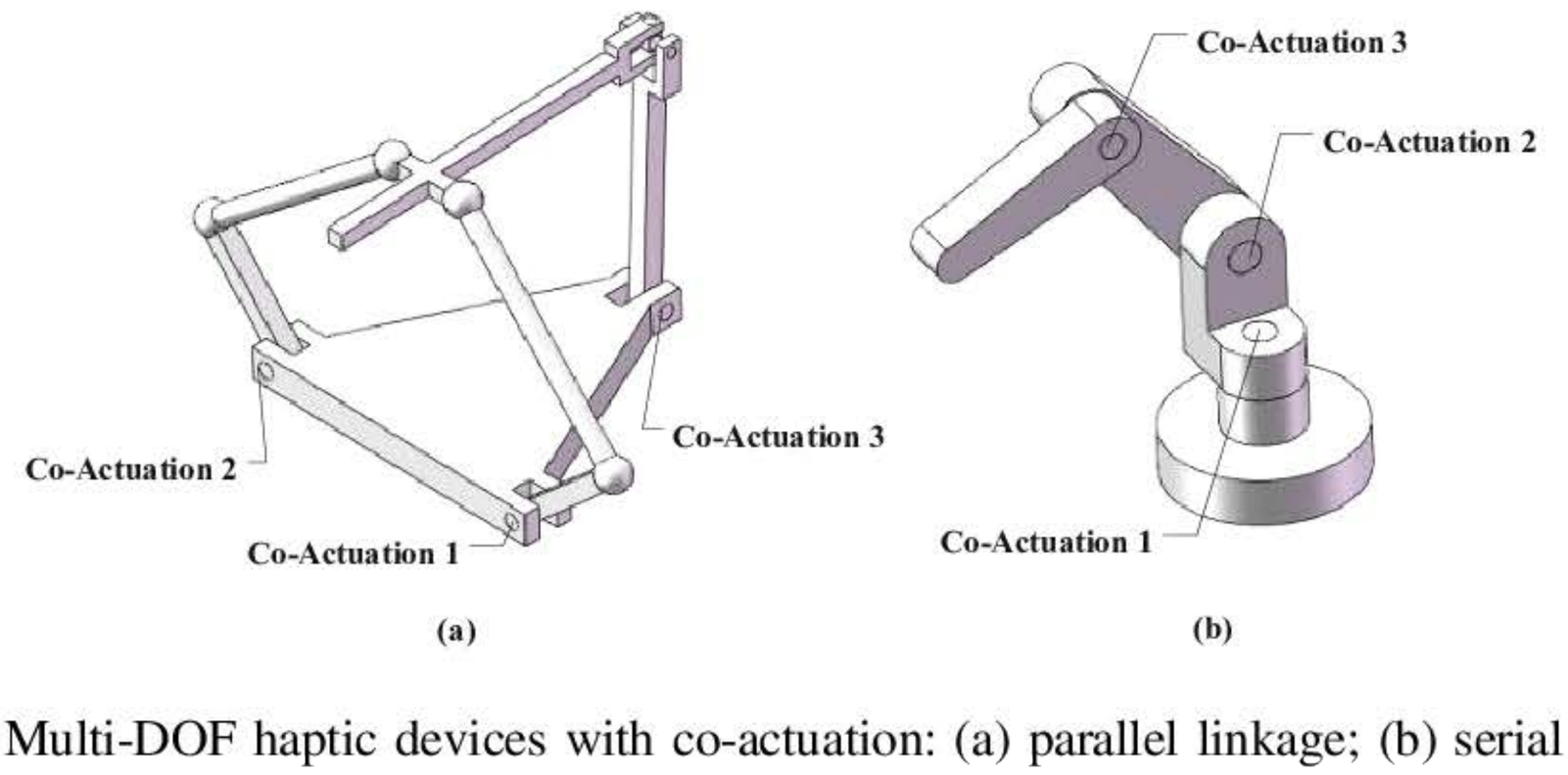

Fig. 9. Multi-DOF haptic devices with co-actuation: (a) parallel linkage; (b) serial linkage

8 Conclusion

We have presented a new concept of co-actuation for reducing inertia and friction in conventional admittance displays. The effectiveness of the approach was tested on a physical prototype of 1-DOF haptic device. The experimental data showed that the

proposed approach can achieve high stiffness while effectively reduce inertia and friction, thus has potential advantage over conventional admittance display.

The clearance between the physical constraint and the link depends on the speed of device and parameters of motor, gear train and controller. A large speed of device requires a large clearance. On the other hand, a small clearance is required for small surface penetration. A key design issue in co-actuation approach is to balance the conflict between fast moving in free space and small penetration in constraint space. Optimal solution to the tradeoff between the two conflict requirements needs to be explored in future study. Concerning our target application of dental simulation, penetration of less than what we obtained in the test may be expected. Our future work will try to find out if the co-actuation approach can achieve the smallest penetration depth required and if haptic illusion can be used to obtain desired performance. In the future, it is also needed to measure the force generation error of the proposed approach. As we adopted the admittance control approach in the constrained space, the error might depend on the force sensing accuracy of the force sensor, the accuracy of the position control of the physical constraint during the constrained space, and the value of the stiffness of the simulated virtual wall.

In the co-actuation approach, because joints are separated from actuators, the compensation of link gravity and inertia is not as easy as in conventional admittance display. Therefore, the approach is suited to the application requiring small workspace, such as VR-based dental simulator. The approach is also applicable to the cases that are more sensitive to large stiffness or force, but less sensitive to device gravity and inertia. Such applications may include virtual fixture in orthopedic surgery, where preventing surface penetration is the most import performance, and rehabilitation, where large force may be required for arm or leg training.

References

1. Massie, T., Salisbury, J.: The PHANTOM haptic interface: a device for probing virtual objects. In: ASME Winter Annual Meeting, Symposium on Haptic Interfaces for Virtual Environment and Teleoperator Systems, vol. DSC 55, Chicago, IL, pp. 295–302 (1994)
2. Salisbury, K., Eberman, B., Levin, M., Townsend, W.: The design and control of an experimental whole-arm manipulator. In: The Fifth International Symposium on Robotics Research, pp. 233–241 (1990)
3. Van der Linde, R., Lammertse, P., Frederiksen, E., Ruiter, B.: The haptic master, a new high-performance haptic interface. In: Proceedings of Euro-Haptics, Edinburgh, U.K. (2002)
4. Faulring, E., Colgate, J., Peshkin, M.: The cobotic hand controller: design, control and performance of a novel haptic display. Int. J. Robot. Res. **25**(11), 1099–1119 (2005)
5. Arata, J., Kondo, H., Ikedo, N., Fujimoto, H.: Haptic device using a newly developed redundant parallel mechanism. IEEE Trans. Robot. **27**(2), 201–214 (2011)
6. http://www.geomagic.com/en/products-landing-pages/haptic
7. Wang, D., Zhang, Y., Hou, J., Wang, Y., Lv, P., Chen, Y., Zhao, H.: iDental: a haptic-based dental simulator and its preliminary evaluation. IEEE Trans. Haptics **5**(4), 332–343 (2012)
8. Hungr, N., Roger, B., Hodgson, A.J., Plaskos, C.: Dynamic physical constraints: emulating hard surfaces with high realism. IEEE Trans. Haptics **5**(1), 48–57 (2012)

9. Colgate, J.E., Schenkel, G.: Passivity of a class of sampled data systems: application to haptic interfaces. In: Proceedings of the American Control Conference, pp. 3236–3240 (1994)
10. Abbott, J.J., Okamura, A.M.: Effects of position quantization and sampling rate on virtual wall passivity. IEEE Trans. Robot. **21**(5), 952–964 (2005)
11. Diolaiti, N., Niemeyer, G., Barbagli, F., Salisbury, J.K.: Stability of haptic rendering: discretization, quantization, time delay, and coulomb effects. IEEE Trans. Robot. **22**(2), 256–268 (2006)
12. Mahvash, M., Hayward, V.: High fidelity passive force reflecting virtual environments. IEEE Trans. Robot. **21**(1), 38–46 (2005)
13. Zinn, M., Khatib, O., Roth, B., Salisbury, J.K.: Large workspace haptic devices: a new actuation approach. In: Symposium on Haptic Interfaces for Virtual Environment and Teleoperator Systems, pp. 185–192 (2008)
14. Cho, C., Song, J.-B., Kim, M.: Energy-based control of a haptic device using brakes. IEEE Trans. Syst. Man Cybern. Part B Cybern. **37**(2), 341–349 (2007)
15. Conti, F., Khatib, O., Baur, C.: A hybrid actuation approach for haptic devices. In: World Haptics 2007, pp. 367–372 (2007)
16. An, J., Kwon, D.S.: Stability and performance of haptic interfaces with active/passive actuators theory and experiments. Int. J. Robot. Res. **25**(11), 1121–1136 (2006)
17. Kwon, T.B., Song, J.B.: Force display using a hybrid haptic device composed of motors and brakes. Mechatronics **16**, 249–257 (2006)
18. Swanson, D.K., Book, W.J.: Path-following control for dissipative passive haptic displays. In: Proceedings of the 11th Symposium on Haptic Interfaces for Virtual Environment and Teleoperator Systems, pp. 101–108, March 2003
19. Gosline, A.H.C., Hayward, V.: Eddy current brakes for haptic interfaces: design, identification, and control. IEEE/ASME Trans. Mechatron. **13**(6), 669–677 (2008)
20. Weir, D.W., Colgate, J.E., Peshkin, M.A.: Measuring and increasing Z-width with active electrical damping. In: Proceedings of the Symposium on Haptic Interfaces for Virtual Environment and Teleoperator Systems, pp. 169–175 (2008)
21. Lawrence, D.A., Chapel, J.D.: Performance trade-offs for hand controller design. In: Proceedings of the IEEE International Conference on Robotics and Automation, vol. 4, pp. 3211–3216, May 1994